

Extended confocal microscopy of myocardial laminae and collagen network

A. A. YOUNG, I. J. LEGRICE, M. A. YOUNG & B. H. SMAILL

Department of Physiology, School of Medicine, University of Auckland, Private Bag 92019, Auckland, New Zealand

Key words. Confocal fluorescence microscopy, extended volume image, myocardial blood vessels, myocardial collagen, myocyte organization, picrosirius red, three-dimensional cardiac microstructure.

Summary

Ventricular myocardium has a complex three-dimensional structure which has previously been inferred from two-dimensional images. We describe a technique for imaging the 3D organization of myocytes in conjunction with the collagen network in extended blocks of myocardium. Rat hearts were fixed with Bouin's solution and perfusion-stained with picrosirius red. Transmural blocks from the left ventricular free wall were embedded in Agar 100 resin and mounted securely in an ultramicrotome chuck. Confocal fluorescence laser scanning microscopy was used to obtain 3D images to a depth of 60 μm in a contiguous mosaic across the surface. Approximately 50 μm was then cut off the surface of the block with an ultramicrotome. This sequence was repeated 20 times. Images were assembled and registered in 3D to form an extended volume $3800 \times 800 \times 800 \mu\text{m}^3$ spanning the heart wall from epicardium to endocardium. Examples are given of how digital reslicing and volume rendering methods can be applied to the resulting dataset to provide quantitative structural information about the 3D organization of myocytes, extracellular collagen matrix and blood vessel network of the heart.

Introduction

Quantitative information about the 3D architecture of ventricular myocardium is required for the analysis of myocardial mechanics and activation in normal and pathological hearts (Spotnitz *et al.*, 1974; Dolber & Spach, 1987; Robinson *et al.*, 1988; LeGrice *et al.*, 1995). In particular, we require detailed information about the organization of and spatial relationships between individual myocytes, muscle layers, cardiac connective tissue and blood vessels. To date, myocardial structure has been

studied using predominantly two-dimensional (2D) imaging techniques such as light and polarization microscopy, with transmission or scanning electron microscopy (TEM, SEM) used for higher resolution. These techniques yield important morphological information and have provided insight into the three-dimensional (3D) arrangement of uniformly varying cardiac structures. However, they cannot be used to reconstruct complex spatial relationships as required to fully characterize myocardial architecture. An imaging modality which is ideal for this task is confocal microscopy (Pawley, 1995). This technique enables volume reconstruction from serial optical sections through thick tissue specimens and so provides a powerful method for elucidating complex 3D structure in biological tissues.

Picrosirius red (PSR) has previously been used as a specific stain for collagen types I, II and III. This dye is known to enhance the birefringence of collagen fibres and is also fluorescent in the Texas Red/Rhodamine range (Sweet *et al.*, 1964; Junqueira *et al.*, 1979; Dolber & Spach, 1987; MacKenna *et al.*, 1996). The proposed mechanism of collagen staining is by the interaction between the sulphonic acid groups of sirius red and the basic amino acids of the collagen molecule in the low-pH environment provided by picric acid (Junqueira *et al.*, 1979). PSR does not bind to collagen in a stoichiometric manner (Puchtler *et al.*, 1988) and therefore collagen content cannot be determined by the intensity of PSR fluorescence, although the relative size and morphology of the collagen network can be clearly identified.

Dolber & Spach (1993) have used confocal fluorescence microscopy together with PSR staining to study the 3D morphology of cardiac collagenous structures. Cytoplasmic background fluorescence was reduced after immersion in phosphomolybdic acid (PMA) prior to PSR staining. Although fine endomysial collagen could not be resolved with these methods, perimysial collagenous weaves and

Correspondence to: A. A. Young. Tel: (649) 3737599; fax: (649) 3737499; e-mail: a.young@auckland.ac.nz

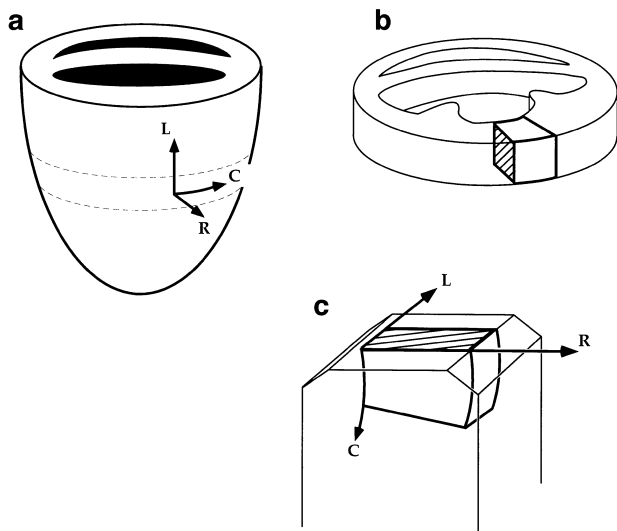


Fig. 1. Schematic showing the location and orientation of LV tissue block. (a) Equatorial ring (dashed lines) excised from the heart. (b) Segment cut from lateral LV free wall between the papillary muscles. (c) Tissue block set in resin mould. Cardiac coordinate system: C – circumferential direction, L – longitudinal direction, R – radial direction. Note that the cross-hatched L–R (longitudinal–radial) surface which is vertical in (b) is uppermost in (c).

ords were clearly identified. Their immersion staining technique allows optical sections to be acquired up to $10\ \mu\text{m}$ deep into the tissue with acceptable signal-to-noise ratio (SNR). However, this is inadequate for a quantitative 3D analysis of the laminar architecture of myocardium and its relationship to the collagen network, since the width of a typical muscle layer is $50\ \mu\text{m}$ and large-diameter collagen fibres can extend over significant distances (several myocyte lengths) before branching (Robinson *et al.*, 1988).

This paper presents a technique for tissue processing and extended 3D visualization of blocks of ventricular myocardium. The technique employs Langendorff perfusion for tissue fixation and staining, TEM tissue preparation methods, optical and physical serial sectioning and computer image processing. A block of rat left ventricular (LV) tissue spanning from epicardium to endocardium was reconstructed in 3D from registered serial optical sections, resulting in a transmural image $3800 \times 800 \times 800\ \mu\text{m}^3$ in volume at a resolution of $1.56\ \mu\text{m}$ per (cubic) voxel side. The distribution and morphology of myofibres, collagen, extracellular spaces and major vessels within this block were examined and compared with previous results from studies which used 2D techniques (light and polarization microscopy, TEM and SEM). Finally, estimates of collagen dimensions made using extended confocal microscopy were compared with measurements of the same structures in TEM images at identical sites.

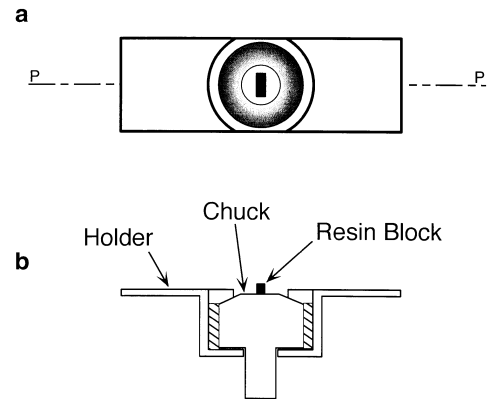


Fig. 2. Mounting assembly showing the resin block fixed in an ultramicrotome chuck and glued into a plastic holder shaped like a microscope slide. (a) Plan view. (b) Section through PP. Hatched region indicates glue.

Methods

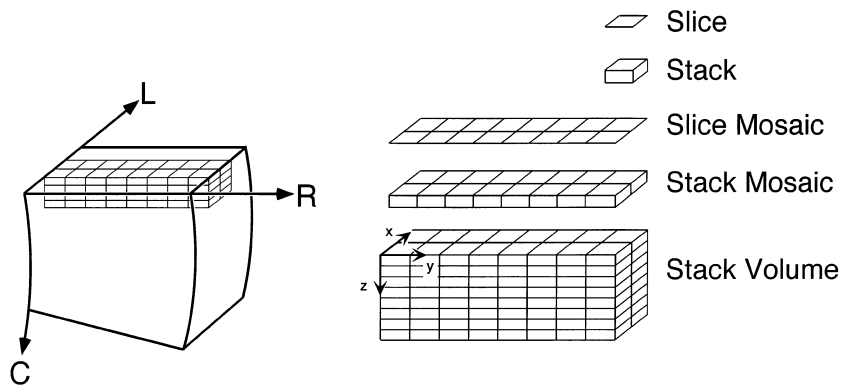
Staining

Experimental protocols were approved by the University of Auckland Animal Ethical Committee. Adult Wistar rats were anaesthetized with 3% halothane in oxygen. Hearts were rapidly excised and arrested by immersion in chilled cardioplegic solution (St Thomas' Hospital Solution 1). The aorta was mounted on a cannula for Langendorff perfusion. Warm (37°C) oxygenated Krebs–Henseleit buffer was used to re-establish spontaneous heart rhythm and when a maximal rate (typically $200\ \text{beats min}^{-1}$) was achieved diastolic arrest was induced by switching the perfusate to St Thomas' Hospital Solution 1 (Robinson *et al.*, 1984). Hearts were then perfused with Bouin's fixative for 15 min, followed by PMA (2.5% aqueous solution) for a further 15 min and finally picosirius red (PSR: 0.1% solution of sirius red F3–BA in saturated aqueous picric acid, $\text{pH} \approx 2$) at $1\ \text{mL min}^{-1}$ for approximately 2 h. In some experiments, the PMA step was omitted. Hearts were stored in Bouin's fixative and further processed after 1 week. The above protocol was determined after experimentation with different fixatives and staining procedures. In particular, results were compared with hearts fixed in formaldehyde (3%) and a formaldehyde–glutaraldehyde mixture (1.5% each).

Embedding

An equatorial ring $\approx 2\ \text{mm}$ thick was removed from the ventricles (Fig. 1a). From this, a transmural segment of LV free wall $\approx 2\ \text{mm}$ wide was cut between the papillary muscles (Fig. 1b). The tissue segment was dehydrated in graded ethanols (70, 80, 95, 100, 100%) and then in propylene oxide, each step being 45 min in duration. The tissue was infiltrated with a 50:50 mix of propylene oxide

Fig. 3. Schematic indicating the three-dimensional organization of the image volume in relation to the specimen. The volume is assembled from an array of contiguous image stacks each consisting of 40 slices (optical sections). The axes LCR represent the cardiac coordinate system, while the xyz axes represent the imaging coordinate system.



and Agar 100 resin (45 min) and then immersed overnight in 100% resin. The infiltrated segment was flat embedded for imaging in the longitudinal–radial (L–R) plane (Fig. 1c) and polymerized at 60 °C for 48 h. Some tissue sections were also mounted in glycerol or Clearium™ for comparison.

Mounting

The tissue block was tightly secured in a Reichert–Jung ultramicrotome chuck with the L–R surface orientated parallel to the base. The chuck was fitted into a custom-made Perspex holder as shown in Fig. 2. This was designed (i) to fit into the slide recess of the microscope stage, (ii) to position the upper surface of the block approximately in the plane of the stage and (iii) to fit interchangeably into the microtome and the microscope stage. The chuck was glued to the holder to guarantee reproducible positioning of the specimen in the microscope.

Confocal imaging and tissue sectioning

The block was trimmed to expose the tissue surface, which was imaged using a Leica TCS 4D Kr–Ar confocal laser scanning microscope (CLSM). A local coordinate system (see Fig. 3) was defined in which the x and y directions were parallel to the microscope imaging plane aligned with the longitudinal and radial directions, respectively, in the heart, and the z direction was vertical (perpendicular to the imaging plane in the circumferential direction). A stepper-motor-driven stage (nominally accurate to 1 μm) allowed translation in the x and y directions of up to 30 mm, using either a manual joystick or software command. Initially, the four upper corners of the block were imaged in reflectance mode to assess the orientation of the surface with respect to the imaging plane. A 10- μm vertical (z) displacement between diagonal corners was deemed acceptable. Otherwise, the block surface was trimmed using a glass knife with the angle settings on the microtome altered to ensure sectioning parallel to the imaging plane. Once set, the ultramicrotome settings were fixed for all further sectioning.

The Leica CLSM uses a mirror scanning system to acquire the image in the x and y directions, and a stage tilt mechanism to acquire the optical section planes. As the stage tilts the specimen may move in the y direction. This movement is zero if the image plane is co-planar with the stage; however, it increases the further the image plane is above or below the stage. In order to avoid the distortions inherent in this tilt mechanism the specimen was held so that the top surface of the resin block was approximately at the level of the microscope stage (see Fig. 2). We estimated that the tilt mechanism contributed up to 5% error over the extent of the reconstructed volume, with variations within this range depending on the position of the image plane relative to the stage.

Confocal images of the embedded specimen were acquired without a coverslip using a 25 \times oil-immersion lens (NA 0.75). A Rhodamine/Texas Red filter set (568 nm excitation wavelength, >590 nm detection filter) was employed, with the pinhole set at 11 optical units. Eight line averages were performed. With these settings optical sections with acceptable SNR could be obtained up to a depth of 60–80 μm .

We adopt the following nomenclature to describe different components of the imaging and registration process (see Fig. 3): ‘slice’ denotes a single optical section, ‘stack’ refers to a single 3D acquisition of 40 optical sections. A ‘slice mosaic’ refers to a set of slices at the same z location (or lateral plane) and a ‘stack mosaic’ refers to a set of stacks obtained at the same z location (i.e. covering the same range of lateral planes). Finally a ‘stack volume’ refers to an extended 3D image data set built up from a series of stack mosaics.

Stacks comprising 40 optical sections, each with a 400 \times 400- μm field of view and 256 \times 256-pixel image matrix, were obtained through a depth of 62.5 μm . This imaging geometry resulted in cubic voxels (1.56 μm per side), which are preferred for digital reslicing and volume rendering. Although undersampled in the lateral plane, the axial resolution was comparable to the FWHM response of the microscope in this direction. The gain of the photomultiplier was manually adjusted with depth

during the acquisition to compensate for the progressive loss of signal in deeper slices. Contiguous 3D stacks (with a small overlap) were acquired by sequentially translating the stage through 392 μm in x and y directions (see Fig. 3). Immediately after acquisition of a stack, a printout of the middle slice was obtained and incorporated into a hard-copy slice mosaic to ensure that there were no errors in the translation sequence. The bottom slice of each corner of the stack mosaic was also printed and used to reposition the stage after each trimming step.

Once imaging of a stack mosaic was complete, the top 40–50 μm of the block was trimmed off with a glass knife in the Reichert–Jung ultramicrotome. The block was then returned to the microscope and repositioned by matching newly acquired images with the printouts of the bottom corner images from the previous stack mosaic. The overlap of at least 12 μm in the z direction provided a safety margin against overtrimming. Imaging and trimming cycles were repeated until a total of 20 overlapping stack mosaics were obtained to a total depth of $\approx 800 \mu\text{m}$.

3D digital registration

The 3D stacks were registered by calculating the x , y , z offset of each stack with respect to the origin. This was done using custom software using the OpenGL library on a Silicon Graphics workstation, making use of accelerated rendering hardware. Within a stack mosaic, individual stacks were registered relative to one corner. Since each stack mosaic was imaged in a single session, there was no movement in the z direction and neighbouring stacks could be aligned by translational offsets in the x and y directions only. Software was written to adjust adjacent stacks in x and y until structural elements (collagen cords and cell boundaries) were matched across slice boundaries. Registration between stack mosaics was carried out as follows. The x , y and z offsets of the four corners of adjacent stack mosaics were determined by matching 3D structure in overlapping regions of the corner stacks. Linear interpolation was then used to calculate offsets for the intermediate stacks.

The offsets determined above were used to assemble the stack volume as a fully registered 3D image. In regions of overlap, only the upper slices from the lower stack mosaic were retained since these had superior SNR. The stack volume was partitioned and archived on magneto-optical disc. In order to visualize the entire imaged volume at once, a reduced resolution stack volume was generated in which each voxel was the average of a $3 \times 3 \times 3$ -voxel neighbourhood in the original image.

Image segmentation

In order to aid visualization of the 3D arrangement of myocytes and collagen, the registered images were

processed using the public domain NIH Image program (developed at the US National Institutes of Health and available on the Internet at <http://rsb.info.nih.gov/nih-image/>). Signal due to collagen was separated from that due to both myocytes and background on the basis of signal intensity and grey-scale morphology. Slices were initially segmented using high- and low-intensity thresholds chosen to label collagen and background unambiguously. However, there was considerable overlap of intensity for myocytes and collagen between these thresholds. The 'rolling ball' background subtraction algorithm of NIH Image (a spatial high-pass filter) was employed to select fine structure above a certain threshold in intensity, which was also labelled as collagen. All collagen pixels were linearly mapped into the grey-scale range 128–255, while pixels labelled background were mapped into the range 0–29. Pixels which were neither collagen nor background were labelled as myocytes and mapped into the grey-scale range 30–127.

Accuracy of depth measurement

In confocal microscopy, resolution and scaling in the z direction usually differs from that in the x – y plane. Spherical aberration, due to mismatch between the refractive indices of the embedding media and the immersion oil, degrades image resolution and introduces a scaling in the z direction (Hell *et al.*, 1993). These issues were investigated in a number of ways. Firstly, the refractive index of the resin was measured using a refractometer. Secondly, the effect of the embedding medium on depth measurement was determined by imaging two thin metal strips offset and glued to each other and fixed to a glass slide. The difference in heights between the top of the two strips was measured using the same oil-immersion lens before and after embedding in resin. Finally, the anisotropy of image acquisition was directly measured in resin-embedded tissue by comparing images obtained in different orientations. A block was positioned for imaging in the circumferential–longitudinal (C–L) aspect and a $400 \times 400 \times 40$ - μm stack was acquired. The tissue block was then rotated 90° in the chuck and imaged in the circumferential–radial (C–R) plane. An extended series of C–R stack mosaics was acquired and registered as described above. This stack volume was then digitally resliced in the C–L plane, allowing comparison of the dimensions of structures imaged in the two orthogonal planes.

Accuracy of collagen dimension measurement

In order to determine the accuracy of estimates of collagen bundle diameter from confocal micrographs, comparisons were made between images of the same bundles as seen in the confocal microscope and the TEM. A region on the

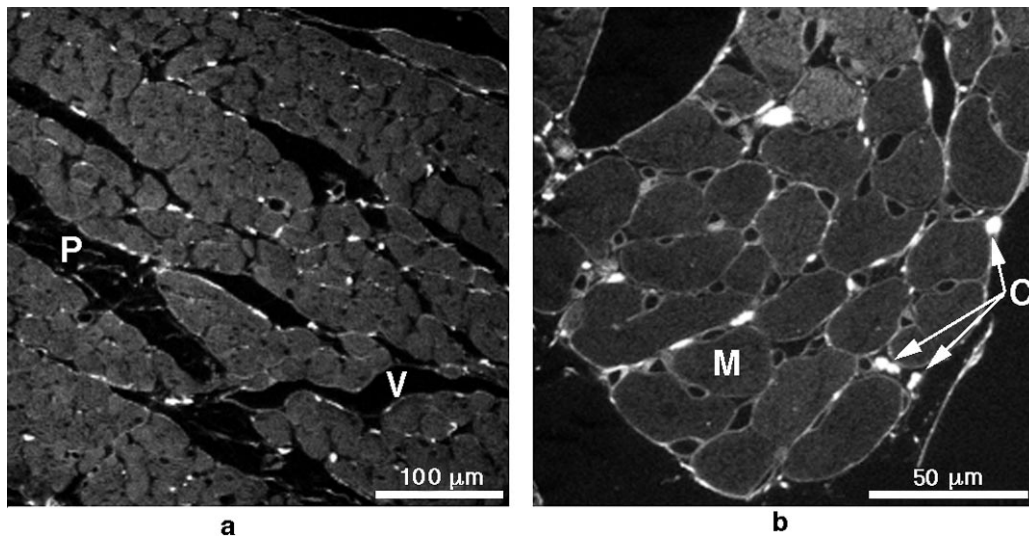


Fig. 4. Image slices from LV midwall. (a) Typical slice from PMA-treated specimen: 25 \times objective, 256 \times 256-pixel image of 400 \times 400- μ m field. (b) Higher magnification image from non-PMA-treated specimen: 63 \times objective, 512 \times 512-pixel image of 150 \times 150- μ m field. Endomysial collagen surrounding individual myocytes is evident. Myocytes (M), collagen cords (C), vascular structures (V) and cleavage planes (P) are indicated.

surface of the block $\approx 1500 \times 1500 \mu\text{m}$ in size was selected for investigation and imaged with the confocal microscope using the 25 \times oil-immersion lens. Areas containing large collagen bundles were then selected for further imaging to a depth of 20 μm with the 63 \times oil-immersion lens. Ultrathin sections ($\approx 90 \text{ nm}$) were cut from the surface of the block and prepared for transmission electron microscopy. Sections were picked up on Formvar-coated slot grids, treated with uranyl acetate and lead citrate, and collagen enhanced with tannic acid. One of the ultrathin sections was then viewed in the TEM (Philips 410) and the collagen bundles selected previously were identified and then recorded at high magnification (2000–9000 \times). The confocal stack containing each collagen bundle was then re-examined in order to identify the slice which most closely matched the plane of the TEM image containing that bundle. Corresponding maximum and minimum diameters were then determined for each collagen bundle using NIH Image software and the relative differences calculated.

Results

Results describing the development of the technique are presented from a number of experiments, together with an extended volume image of LV myocardium obtained from a single heart.

Staining

Figure 4(a) shows a typical slice taken from a midwall region of a transmural LV free wall block at 25 \times magnification. A higher power (63 \times lens) image of a similar

region is shown in Fig. 4(b). Staining was uniform throughout the heart wall in all cases where the perfusion procedure was successful. Collagen staining with PSR was best following fixation with Bouin's solution. Formaldehyde-fixed hearts did not stain well for collagen while glutaraldehyde fixation led to excessive autofluorescence. For Bouin's-fixed hearts examined immediately after perfusion, PSR was found to be concentrated in the capillary endothelial cell nuclei. Maximal collagen staining was only achieved 3–5 days after perfusion. Stained tissue was therefore stored in Bouin's solution for this period prior to embedding in resin.

Resin-embedded tissue had a similar appearance to sections mounted in glycerol or CleariumTM; however, the signal intensity from myocytes was higher in resin-embedded specimens. For sections subsequently mounted in glycerol or Clearium, pre-PSR treatment with PMA reduced the myocyte signal. This was not observed in resin-embedded tissue, in which the only apparent effect of PMA was to reduce the signal from the endomysial collagen. Endomysial collagen was most evident in higher magnification images and was clearly seen in non-PMA-treated tissue (Fig. 4b). HCl treatment after staining with PSR has previously been used to improve the collagen signal in mounted sections (Dolber & Spach, 1993) but we did not observe any difference with HCl treatment in resin-embedded tissue.

Registration

The overlap in the x and y directions between adjacent stacks in the same stack mosaic was consistently 2–5

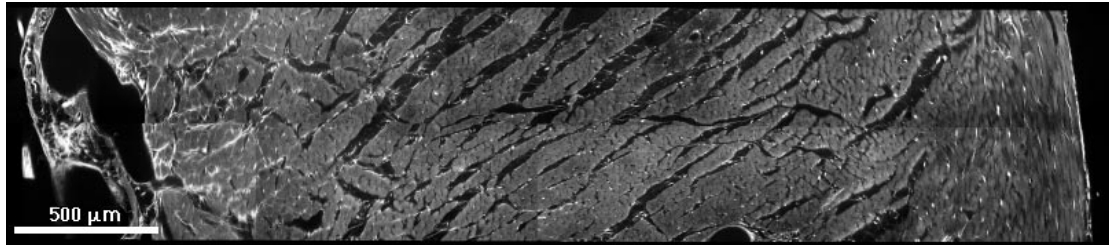


Fig. 5. Slice mosaic through the registered stack volume spanning the heart wall from epicardium to endocardium.

pixels. However, the overlap in the z direction between adjacent stacks was more variable (up to 15 voxels). All stacks could be registered to the nearest voxel by matching collagen structures in the overlapping regions. Figure 5 is a fully registered extended 2D image (slice mosaic) spanning the LV wall from epicardium to endocardium. Figure 6 is a rendered 3D projection showing the entire stack volume spanning $3600 \times 800 \times 800 \mu\text{m}$. It is evident that this provides a coherent view of the 3D organization of ventricular myocardium. The slightly striated texture of the front surface is due to variation in intensity with depth in each stack. This was minimized by progressive adjustment of photomultiplier gain during each 3D acquisition.

Three-dimensional organization of ventricular myocardium

Figure 6 provides a macroscopic view of the 3D organization of ventricular myocardium. The top and front faces of the reconstructed volume are (in cardiac coordinates) the L–R and C–R aspects of the block. The most striking features of this 3D image are the laminar organization of myocytes and the extensive cleavage planes between layers. When viewed from the L–R aspect, the layers have an approximately radial orientation, becoming more longitudinal in the

subendocardial and subepicardial regions, with a chevron or pinnation pattern in the C–R aspect. These orientations are consistent with those seen previously in rats and dogs using 2D techniques (Hort, 1960; Spotnitz *et al.*, 1974; LeGrice *et al.*, 1995). Connective tissue (white) is organized in close association with the muscle layers and apparently increases in density near the epicardial and endocardial surfaces (left and right sides of the figure, respectively). The extensive collagen network covering the epicardial surface is obvious in this figure, as is the convoluted nature of the endocardial surface.

With an extended volume image, such as that presented in Fig. 6, it is possible to investigate local microstructure systematically in its 3D context. Structures observed in 2D extended sections can be interpreted with greater confidence because they may be followed in any direction throughout the adjacent volume using a wide variety of viewing modes. Preliminary results obtained in this way are outlined below.

Myocyte orientation and laminar structure

In Fig. 7, the stack volume has been digitally sectioned approximately parallel to the epicardial surface and 2D views are presented at five representative sites through the



Fig. 6. Three-dimensional representation of the registered stack volume. The longitudinal radial (L–R) surface of the block is uppermost and the front face is the most basal C–R aspect of the block. Epicardial and endocardial surfaces are indicated.

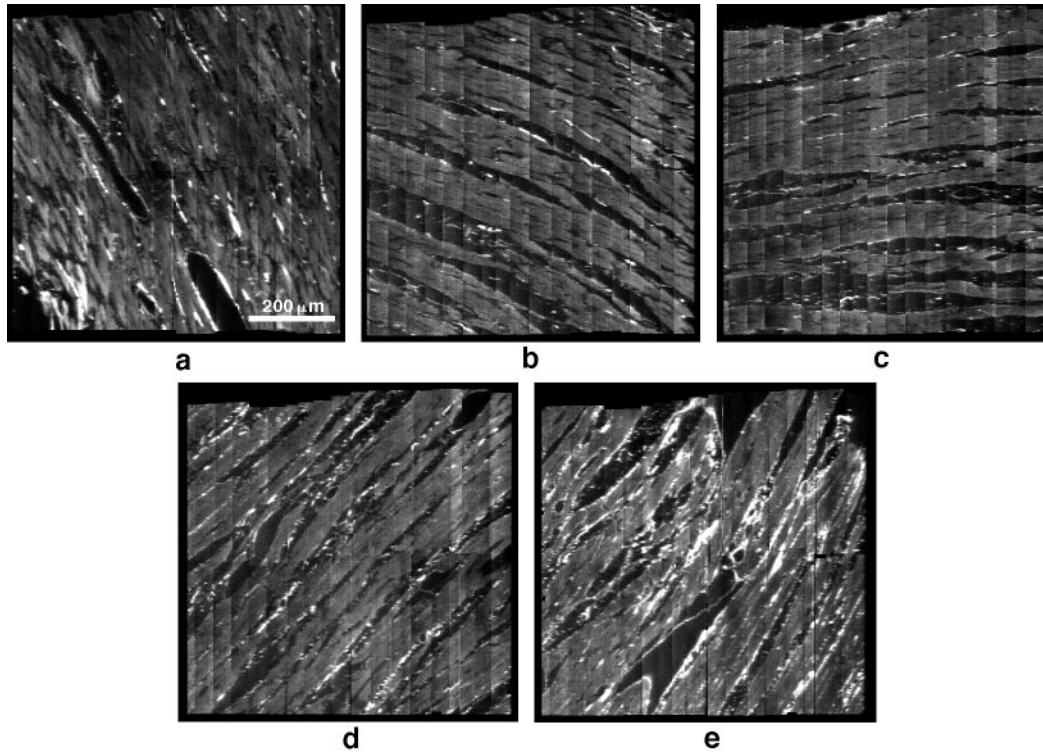


Fig. 7. Transmural variation of muscle layer orientation. The stack volume is digitally sectioned approximately parallel to the epicardial surface at five sites distributed through ventricular wall from subepicardium (a) to subendocardium (e). The transmural location of these sites is indicated by the solid white lines in the corresponding panels a to e in Fig. 8. Note: the right-hand side of each panel in Fig. 7 corresponds to the upper surface of the block.

LV wall. Myocytes in longitudinal section can be identified at this magnification and the laminar arrangement of myocytes is evident. Layers are typically three to four cells thick and muscle bridges between adjacent laminae are relatively sparse. It is evident that there is some reduction of image quality when reslicing an extended confocal volume of this type, due to the reduced resolution in the *z* direction.

The apparent orientation of myocytes (and layers) varied progressively through 120° from subepicardium to subendocardium, in agreement with previous histological results (Streeter, 1979). In the past, the transmural distribution of muscle 'fibre' orientation has been quantified using equivalent histological sections cut parallel to the epicardial tangent plane, assuming that the imbrication angle (the angle between the myocyte axis and the epicardial tangent plane) is negligible (Streeter, 1979). This assumption is tested in Fig. 8, which shows the complete block sectioned in five different orientations (all perpendicular to the epicardial tangent plane) chosen to coincide with muscle layer orientations seen at the five sites shown in Fig. 7. Imbrication angles can therefore be viewed directly at these sites and are negligible in this specimen.

Organization of connective tissue network

Extended confocal microscopy techniques also make it possible to study the 3D arrangement of major elements of the cardiac connective tissue matrix. Networks of collagen cords which span cleavage planes to connect adjacent muscle layers are evident in both Fig. 5 and Fig. 6. Large collagen cords which are aligned approximately with the myocyte axis and extend over many cell lengths are observed in the cleavage planes (Figs. 4–7). There also appears to be a relatively high density of these cords within muscle layers. These longitudinal cords have a convoluted rather than a coiled appearance.

Analysis of the extended volume image also demonstrates the problems inherent in attempts to quantify connective tissue organization from 2D transmural ventricular sections. In Fig. 8(b), the section plane is perpendicular to the myocyte axis at the subendocardial site identified by the broken line, while in Fig. 8(e), the section plane contains the myocyte axis at this site. The appearance of collagen density in these two views is markedly different. In order to make valid comparisons of connective tissue organization at different transmural sites it is therefore necessary to account for local myocyte orientation.

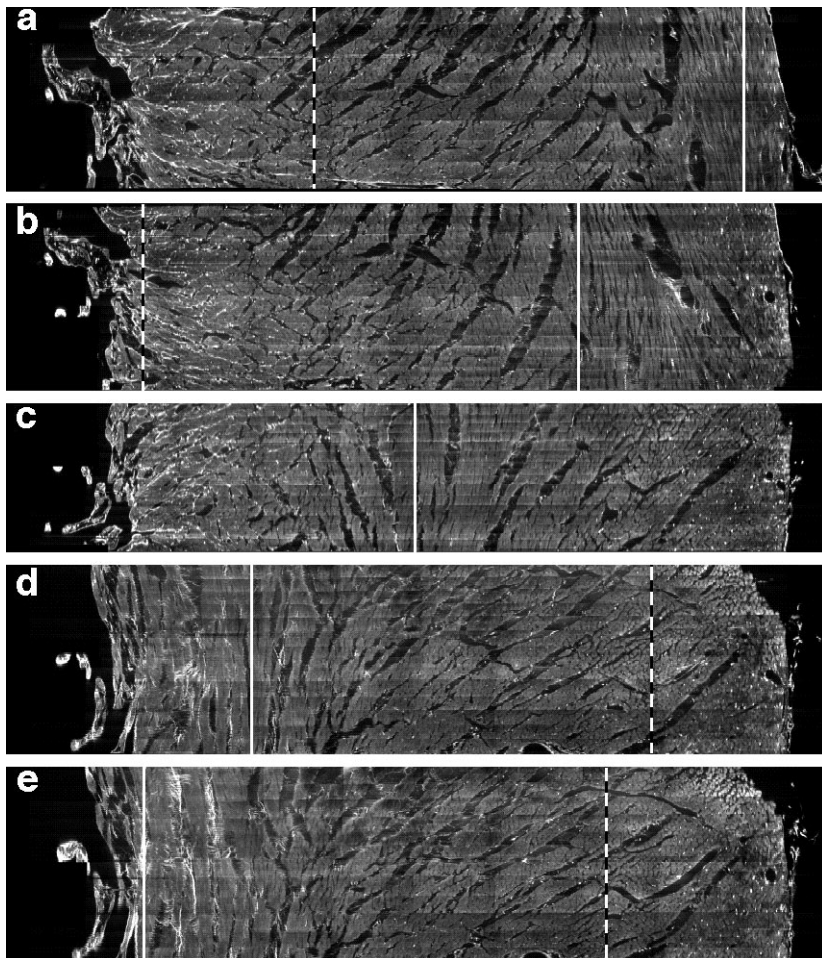


Fig. 8. Transmural variation of imbrication angle and connective tissue organization. The volume is digitally sectioned in five different orientations. Section orientation in (a)–(e) is parallel to the muscle layer orientation in Fig. 7(a–e), respectively. The solid white lines in each panel indicate the positions of corresponding sections in Fig. 7. Thus the solid line in each panel indicates the transmural site at which the myocyte axis is in plane with the section, while broken white lines indicate sites at which the myocyte axis is perpendicular to the section plane.

The 3D organization of the perimysial collagen network and its spatial relationship with the muscle layers is shown in Fig. 9(a,b). Collagen, segmented as outlined in the Methods section, is displayed in the presence and absence of background signal due to myocytes. These rendered 3D projections show the density of the convoluted collagen cords aligned with the myocyte axis and demonstrate that these cords are present within and between muscle layers.

Blood vessel network

Various components of the coronary circulation can be also identified in cleavage planes and muscle layers. Typically, blood vessels are closely associated with the connective tissue matrix and are aligned with the large collagen cords. However, the vascular spaces seen intersecting muscle layers do not follow this pattern. These structures are surprisingly extensive and may traverse several layers. They can be identified by a thin wall which stains lightly with PSR and an interior with no discernible structure (unlike the gaps between laminae, which contain collagen cords).

These vascular sinuses, which can be clearly seen in Figs. 4 and 5, were manually segmented and volume rendered to obtain the 3D projection in Fig. 9(c,d).

Depth measurement validation

The refractive index of the polymerized resin was found to be ≈ 1.52 using a standard refractometer. This matched the refractive index of the immersion oil (1.515). The measured thickness of a metal strip imaged in oil and then in resin differed by an average 5% (with the resin producing slightly greater distances than oil). Similarly, there was good agreement between observed dimensions of structures imaged in two orthogonal orientations. Distances measured between structural features in C–L images from resin-embedded tissue and in equivalent images reconstructed from C–R stacks showed less than 6% difference. These results indicate that the acquired 3D images were approximately isotropic, with no significant distortion in the z direction due to refractive index mismatch.

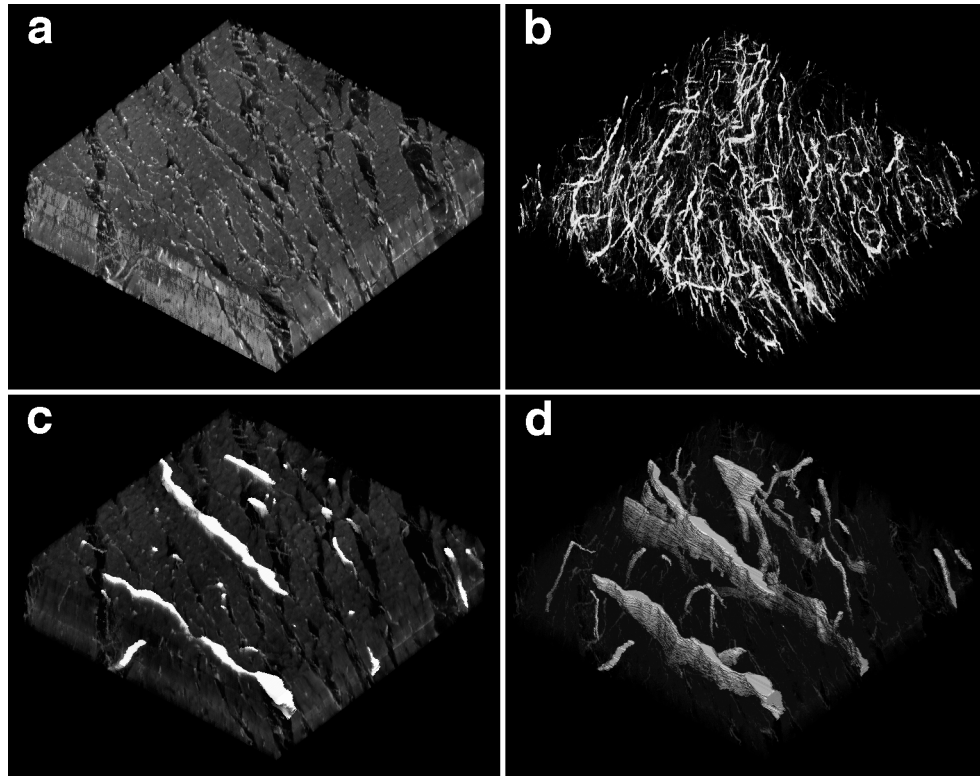


Fig. 9. Three-dimensional representation of segmented subvolumes showing the arrangement of collagen (a,b) and vascular sinuses (c,d). The volume is $800 \times 800 \times 100 \mu\text{m}$. Collagen segmented and rendered (a) in the presence of background signal due to myocytes and (b) with background removed. Manually segmented vascular sinuses rendered (c) in the presence of background signal due to myocytes and (d) with background removed.

Comparison with TEM

Comparison of TEM images with confocal images of the same tissue confirmed that brightly fluorescent structures in the confocal micrographs were collagen. This is illustrated in Fig. 10, where two collagen bundles labelled A and B are seen in cross-section in both the TEM and the confocal images. The resolution of the digitized TEM image was $0.024 \mu\text{m}$, whereas in the confocal image it was $0.31 \mu\text{m}$. Major and minor diameters of bundles A and B are 6.76 , 4.05 , 5.04 and $3.57 \mu\text{m}$ in the TEM image and corresponding measurements in the confocal micrographs are 8.0 , 5.4 , 6.7 and $4.4 \mu\text{m}$. The measurements correspond to overestimates of collagen bundle diameters of 18%, 33%, 33% and 23%. Measurements from confocal images of seven other bundles overestimated collagen bundle diameter by an average of $0.9 \mu\text{m}$ ($23 \pm 16\%$) as compared with TEM images; in no case did the confocal image underestimate collagen bundle dimension.

Discussion

The techniques outlined in this paper provide a framework for quantitative analysis of 3D structure in relatively large

biological specimens. The method employs confocal laser microscopy and was developed to study the arrangement of cardiac myocytes, connective tissue and blood vessels in ventricular myocardium. However, it could be used in a variety of tissues. A repeated sequence of optical and physical sectioning was employed under conditions which enable accurate spatial registration to be preserved. This has enabled us to assemble an extended transmural image of rat ventricular myocardium $3800 \times 800 \times 800 \mu\text{m}^3$ in volume with a resolution of $1.5 \mu\text{m}$ per voxel side. As far as we are aware this is the most extensive data set of this type at present available.

Staining embedding and imaging protocol

We found that it was possible to stain uniformly for collagen throughout thick myocardial specimens by perfusing PSR through the coronary arteries and storing the tissue in Bouin's fixative for at least 3 days prior to resin embedding. Hearts fixed or stored in formalin will not maintain staining as well as hearts fixed and stored in Bouin's fixative. Resin embedding was employed because it provides long-term specimen stability, with reduced distortion under sectioning

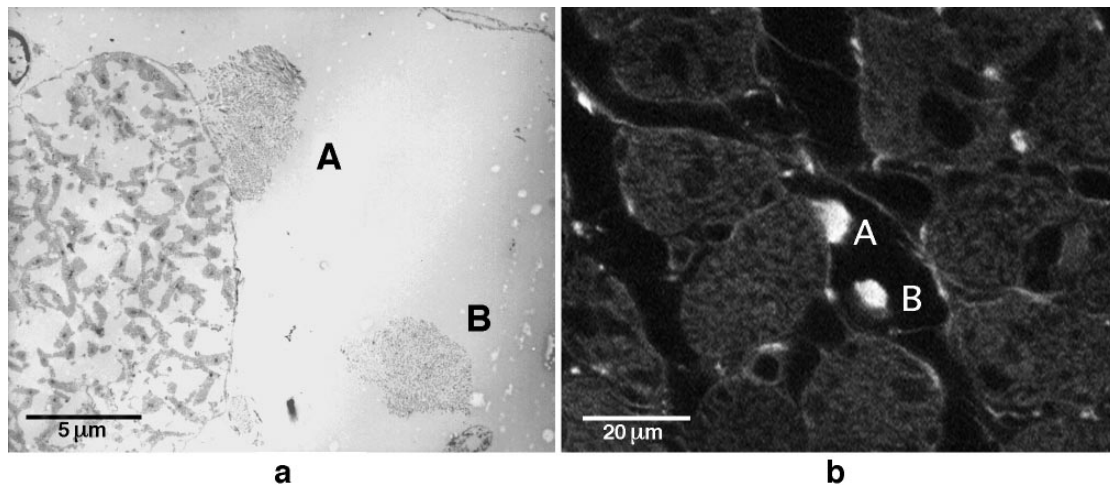


Fig. 10. Comparison of confocal image slice with TEM image of the same structure. (a) TEM image of myocyte (at left-hand margin) and collagen cords (A,B) in cross-section. (b) Confocal image slice at same site. PSR-stained collagen cords are identified by the intensity of fluorescence signal and are labelled appropriately.

and increased imaging depth compared with other mounting methods. Tissue could be imaged with acceptable SNR to a depth of 60–80 μm. The degradation of image quality was probably due to the accumulating effect with depth of absorbance and scattering of light by the tissue.

Phosphomolybdic acid (PMA) has previously been used to minimize the cytoplasmic fluorescence (Dolber & Spach, 1987, 1993). However, in resin-embedded specimens, PMA had little effect on background fluorescence and fine structures such as endomysial collagen could be more clearly identified without PMA treatment. The refractive index of the resin-embedded tissue did not change appreciably when PMA was used, whereas PMA increases the refractive index of mounted tissue sections (Dolber & Spach, 1987). We conclude that the effects of PMA are largely nullified during the dehydration and embedding process. The perfusion and embedding protocol resulted in a greater myocyte signal than in sections mounted in glycerol or Clearium; however, this myocyte signal facilitated analysis of relationships between muscle and connective tissue architecture.

At present, the dimensions of the specimens which can be studied using these techniques are limited by the processing and sectioning methods employed. The cores of large tissue blocks are difficult to dehydrate and embed with resin, and the glass knives used in the ultramicrotome chipped specimens when removing sections more than 2 mm transverse to the knife.

Accuracy of imaging and reconstruction

Cubic voxels were acquired in this study to simplify the processes of 3D image reconstruction, volume rendering

and digital reslicing of the image volume. The sampling density was set to reduce the volume of data acquired while retaining structures of interest such as cardiac myocytes and the perimysial collagen network. Spherical aberration due to mismatch between the refractive indices was minimized and errors in measured dimensions in the *z* direction were thus relatively small.

We found that the motion of the specimen was not exactly specified by the stage scanning software, although with sufficient bonding of the chuck to the holder the error was minimal. An overlap of 5 μm was sufficient to match adjacent 400-μm-wide images. The overlap in the *z* direction between adjacent stacks was more variable (up to 15 voxels) due to the inability to specify accurately the amount of material trimmed by the glass knife. Relative rotations of the image plane due to positioning inaccuracies between imaging sessions were ignored in the reconstruction process; however, structures could be registered to the voxel resolution in all cases, implying that the rotations were very small.

The precision with which collagen dimensions can be measured in PSR-stained myocardial specimens using extended confocal microscopy has been determined by comparing the cross-sectional dimensions of corresponding collagen cords identified in confocal and TEM images. Collagen dimensions are consistently overestimated using fluorescence confocal microscopy. The error is probably due to the greater optical section thickness in the confocal microscope relative to the physical section thickness with TEM and the relatively large pixel size used in the confocal images. This comparison provides a basis for assessing the reliability of collagen dimension measured using fluorescence confocal microscope. However, it should be noted that

the resolution of the confocal images precludes analysis of fine collagen structures.

Measurements of collagen cord diameter may be affected by fixation with Bouin's solution, which can cause collagen swelling. Measurements of myocyte orientation and collagen density may also be affected by tissue shrinkage and distortion in the fixation, dehydration and embedding process. These artefacts are considerably less with resin than with paraffin embedding and can be further minimized by careful dehydration in suitably graded ethanol solutions. Previous studies (Hayat, 1989) report measurement artefacts of less than 10% using the techniques employed here.

In the present application the collagen fibres provided an intrinsic network of fiducial markers which were used to register adjacent overlapping data sets. Since the collagen fibres were not strictly parallel, their relative positions changed appreciably from slice to slice, allowing registration to within a pixel. Registration errors should therefore be relatively random from layer to layer and should not accumulate over large distances. In other applications the use of implanted fiducial markers is required in order to avoid the accumulation of errors. This is a difficult problem since the markers must be small, well defined and structured so as to allow accurate registration in three dimensions.

Collagen and myocyte structure

Rather than provide a detailed description of cardiac microstructure, the purpose of this paper was to describe techniques developed for the 3D analysis of that structure. The results presented demonstrate the advantages of using an appropriate volume data set to analyse the 3D organization of complex biological structures such as ventricular myocardium. They also highlight the need to refer morphological measurements to local coordinate systems which reflect the characteristic microstructure of the tissue studied. Two specific examples are considered below: imbrication angle and collagen density.

The extent of imbrication (orientation of myocyte axis with respect to ventricular surfaces) at different sites within the left ventricle has long been the subject of controversy. Evidence has been presented by Streeter (1979) and co-workers that imbrication angles are present in the LV free wall but are typically less than 10°. Using a transmural volume image, the 3D orientation of myocytes can be reliably determined and imbrication angles may therefore be quantified throughout the ventricular wall. In this paper, the image volume has been sequentially resliced so that the transmural variation of imbrication angle can be visualized. We conclude that imbrication angle was negligible for the one myocardial specimen considered.

We have also shown that the appearance of perimysial components of the cardiac extracellular connective tissue

matrix is very different in planes parallel with and transverse to the local myocyte axis. Clearly, it is necessary to account for this when comparing the organization of perimysial collagen at different sites in the ventricular wall. Within this context, there was a clear transmural variation in the extent and the arrangement of perimysial connective tissue in the one myocardial specimen considered here. There was also a high density of convoluted collagen cords which are aligned with the myocyte axis distributed throughout muscle layers.

Disadvantages of the extended confocal microscopy technique are that it is time-consuming and produces a large amount of data. The reconstruction presented here spans the lateral LV wall of a rat heart and represents a volume of 2.43 mm³. About 2 h was needed to image one stack mosaic. Additional time is required to register the images; however, this step may be automated (Becker *et al.*, 1996). The extended volume consists of 20 stack mosaics and requires 0.5 Gbytes of computer memory. It would be impractical to use this approach to visualize the structural organization of an entire heart in three dimensions. However, the method is well suited to providing precise quantitative information about the 3D arrangement of complex structures in relatively large tissue samples. The techniques described here are currently being used in our laboratory to characterize microstructure at selected sites in the right and left ventricles of rats and to quantify morphological changes associated with the development of hypertrophy in spontaneously hypertensive rats.

References

- Becker, D.E., Ancin, H., Szarowski, D.H., Turner, J.N. & Roysam, B. (1996) Automated 3D montage synthesis from laser-scanning confocal images: Application to quantitative tissue-level cytological analysis. *Cytometry*, **25**, 235–245.
- Dolber, P.C. & Spach, M.S. (1987) Thin collagenous septa in cardiac muscle. *Anat. Record*, **218**, 45–55.
- Dolber, P.C. & Spach, M.S. (1993) Conventional and confocal fluorescence microscopy of collagen fibres in the heart. *J. Histochem. Cytochem.* **41**, 465–469.
- Hayat, M.A. (1989) *Principles and Techniques of Electron Microscopy: Biological Applications*. CRC Press, Boca Raton, Florida.
- Hell, S., Reiner, G., Cremer, C. & Stelzer, E.H.K. (1993) Aberrations in confocal fluorescence microscopy induced by mismatches in refractive index. *J. Microsc.* **169**, 391–405.
- Hort, W. (1960) Makroskopische und mikrometrische Untersuchungen am Myokard verschieden stark gefüllter linker Kamern. *Virchows Arch. Path. Anat.* **333**, 523–564.
- Junqueira, L.C.U., Bignolas, G. & Brentani, R.R. (1979) Picrosirius staining plus polarization microscopy, a specific method for collagen detection in tissue sections. *Histochem. J.* **11**, 447–455.
- LeGrice, I.J., Smail, B.H., Chai, L.Z., Edgar, S.G., Gavin, J.B. & Hunter, P.J. (1995) Laminar structure of the heart: ventricular myocyte arrangement and connective tissue architecture in the dog. *Am. J. Physiol.* **38**, H571–H582

- MacKenna, D.A., Omens, J.H. & Covell, J.W. (1996) Left ventricular perimysial collagen fibers uncoil rather than stretch during diastolic filling. *Basic Res. Cardiol.* **91**, 111–122.
- Pawley, J.B. (ed.) (1995) *Handbook of Biological Confocal Microscopy*. Plenum Press, New York.
- Puchtler, H., Meloan, S.N. & Waldrop, F.S. (1988) Are picro-dye reactions for collagens quantitative? *Histochemistry*, **88**, 243–256.
- Robinson, L.A., Braimbridge, M.V. & Hearse, D.J. (1984) Comparison of the protective properties of four clinical crystalloid cardioplegic solutions in the rat heart. *Ann. Thoracic Surg.* **38**, 268–274.
- Robinson, T.F., Geraci, M.A., Sonnenblick, E.H. & Factor, S.M. (1988) Coiled perimysial fibers of papillary muscle in rat heart: morphology, distribution, and changes in configuration. *Circ. Res.* **63**, 577–592.
- Spotnitz, H.M., Spotnitz, W.D., Cottrell, T.S., Spiro, D. & Sonnenblick, E.H. (1974) Cellular basis for volume related wall thickness changes in the rat left ventricle. *J. Mol. Cell. Cardiol.* **6**, 317–331.
- Streeter, D.D. (1979) Gross morphology and fiber geometry of the heart. *Handbook of Physiology* (ed. by R. M. Berne, N. Sperelakis and S. R. Geigert), Vol. 1, pp. 61–112. American Physiological Society, Williams and Wilkins Company, Baltimore.
- Sweat, F., Puchtler, H. & Rosenthal, S.I. (1964) Sirius red F3BA as stain for connective tissue. *Arch. Pathol.* **78**, 69–72.